2024 International Symposium on Electromagnetic Compatibility – EMC Europe | 979-8-3503-0735-1/24/$31.00 ©2024 IEEE | DOI: 10.1109/EMCEurope59828.2024.10722326

Analysis of Conducted Emission with influences of operating frequencies and amplitudes of a self-oscillating capacitive touch sensing circuit

Subramaniam Saravana Sankar[1], Stanislav Kovar[1], John F. Dawson[2], Michael Galda[3]

[1]Department of Security Engineering, Faculty of Applied Informatics, Tomas Bata University in Zlin, Czech Republic

[2]School of Physics Engineering and Technology, University of York, UK

[3]Systems Engineering, NXP Semiconductors, Czech Republic

{saravana_sankar, skovar}@utb.cz, john.dawson@york.ac.uk, michael.galda@nxp.com

***Abstract* — In the rapidly evolving field of human-machine interfaces (HMI), particularly in the realm of touch screen technologies, capacitive touch sensing has gained prominence due to its superior flexibility and cost-effectiveness compared to other touch interfaces, such as resistive-based methods, infrared touch sensors, and surface acoustic wave sensors. However, this advancement comes with increased emission and susceptibility to Electromagnetic Interference (EMI) and similar disturbances, notably due to factors like operating sensing frequency and voltage. The previous research underscored the challenges of Electromagnetic Emission and some drawbacks of operating capacitive sensors at higher excitation frequencies. Characteristics of traditional capacitance to digital circuits like sigma-delta capacitive sensing circuits operate at higher frequencies, thus producing challenges in terms of emission and susceptibility. This paper offers a detailed assessment of the conducted electromagnetic emissions in a self-oscillating capacitance-to-time converter. The study primarily investigates how conducted emission characteristics change in response to the sensing circuit's operating frequency and voltage variations. The oscillating capacitive sensing circuit conducts sensing with a single clock cycle, thus mitigating some of the issues associated with the traditional capacitive sensing circuits, such as sigma-delta capacitive sensing, which generally require a higher frequency of operations. The results indicate that as the sensing frequency and the operating voltage decrease, the conducted emission of the sensor improves; this phenomenon can be particularly beneficial in high EMI environments like the automotive industry, where capacitive touch sensors are placed close to sensitive electronics.**

***Keywords* — Conducted Emission, Frequency Domain Analysis, Time Domain Analysis, Time-Frequency Domain Analysis.**

I. INTRODUCTION

Touch-sensing technology is pivotal in various applications, especially in consumer electronics such as smartphones, tablets, and laptops. This technology can be broadly classified into resistive-based, infrared sensing, surface acoustic wave sensing, and capacitive touch sensing. In general, two types of touch sensing are widely used, i.e., Resistive touch sensing, which operates by detecting voltage changes across a resistor due to the touch action, and capacitive touch sensing, which measures variations in capacitance caused by a touch action [1], [2]. Among the two, capacitive touch sensing, recognized for its cost-effectiveness and adaptability, is more prevalently used than resistive-based touch sensing in consumer electronics and HMI within the automotive industry[3], [4]. Capacitive sensing is further divided into self-capacitance and mutual capacitance-based touch sensing, as illustrated in Fig. 1. Fig. 2 shows the general working process of both types of capacitive sensing.

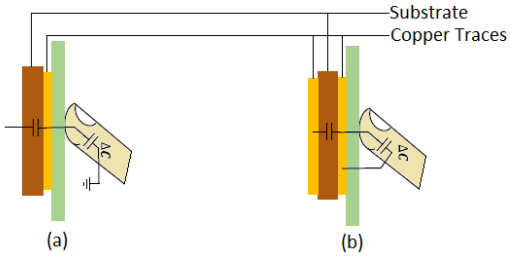

Fig. 1. (a) Self-Capacitance based touch sensing (b) Mutual-Capacitance based touch sensing.

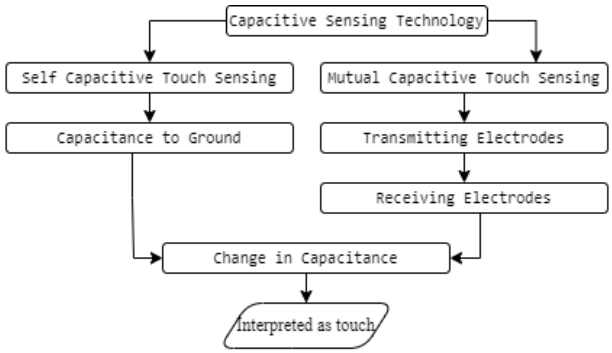

Fig. 2. General working flow of capacitive touch sensing.

Capacitive touch sensing is particularly vulnerable to conducted and radiated EMI, a problem that is exacerbated as the sensing frequency rises. For instance, researchers have observed touchscreen malfunctions in consumer devices caused by minute, i.e., a few µA common-mode (CM) currents originating from power adapters [5].

This project has received funding from the European Union's Horizon Europe research and innovation program under the Marie Sklodowska-Curie grant agreement No. 101072881 and UKRI.

In capacitive touch sensing, the traditional method to measure change in capacitance involves sending small discrete charge packets to the sensor capacitor and comparing the total number of charge packets required to charge the sensing capacitor against a reference capacitor [6], [7], [8]. The sigma-delta sensing circuit is a prime example of this technique. The speed and resolution of this method are closely tied to the operating frequency, where operating frequency is directly proportional to the sensing speed, which poses challenges in terms of EMI/EMC [9], [10].

This paper presents an analysis of the conducted emission by a self-oscillating capacitive sensing circuit, and the influence of operating frequency and amplitude is also shown. Unlike the traditional sensing circuit, the proposed circuit uses a single oscillating cycle to do sensing, in which the speed and resolution depend on the change in the duty cycle.

The rest of this paper is arranged as follows: Section II details the working of the sensing circuit. Section III discusses the analysis of the conducted emission. Section IV examines conclusions on the results.

II. Experimental Setup and Procedures for Evaluating Conducted Emission

A. Principle and working of an Oscillating Capacitive Sensing Circuit

Fig. 3 demonstrates a design for an oscillating capacitive sensing circuit. Central to this circuit is a relaxation oscillator, similar to the one discussed in [11]. The relationship between the sensing capacitance, denoted as C_{sen}, and the output voltage, V_{do}, is described by equations (1)-(5) where T_{on}, T_{off}, and f_{osc}, represent the duration of the oscillator's on-time, off-time, and its oscillation frequency, respectively.

$$K = R_1/R_2 \quad (1)$$

$$J = (C_{sen} - C_{off})/C_{Int} \quad (2)$$

$$T_{on} = R_{ref} * C_{Int} * K \quad (3)$$

$$T_{off} = R_{ref} * C_{Int} * (K - 2J) \quad (4)$$

$$f_{osc} = 1/(T_{on} + T_{off}) \quad (5)$$

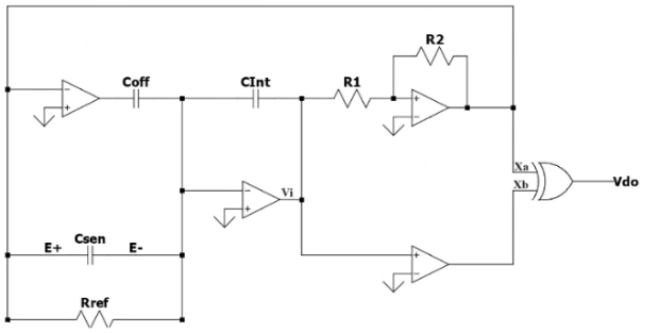

Fig. 3 Self-Oscillating Capacitive touch sensing circuit.

This study focuses on how the circuit performs with varying combinations of operating voltages and frequencies. Table 1 and Table 2 provide an outline of the operational settings tested with the sensing circuit. Fig. 4 displays the output V_{do} waveform during the touched and untouched events, captured under the operating conditions characterized by 0.59kHz and 5V. The proposed circuit is fabricated on a Printed Circuit Board (PCB) as shown in the Fig. 5.

Table 1 Operating Frequencies of Sensing Circuit

Frequency (in kHz)	34.1	20.0	10.9	5.7	4.2	2.3	1.0	0.93	0.7	0.59

Table 2 Operating Voltages of Sensing Circuit

Peak to Peak Voltage	5.0	4.5	4.0	3.5	3.0	2.5

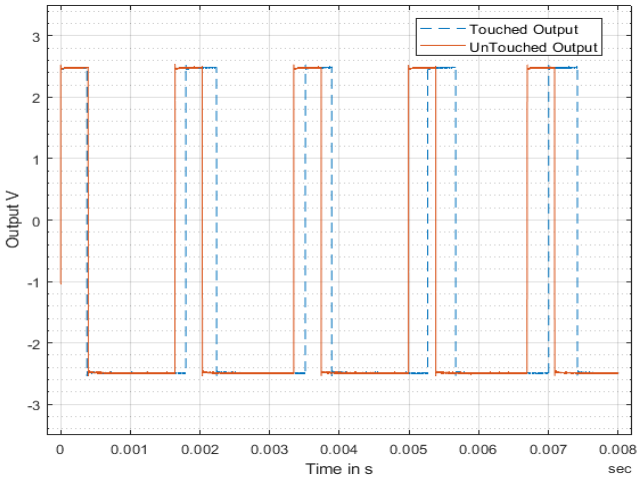

Fig. 4 Output V_{do} waveform from sensing circuit at 0.59kHz and 5V.

B. Procedure and Experimental Setup of Conducted Emission

The conducted emission measurement setup used in this study is illustrated in Fig. 6; like the work in [12], [13]. It utilizes a 5uH LISN (Model: NNBM 8124) from SCHWARZBECK, and EMI Test Receiver (ESPI-7), and a Time Domain Oscilloscope (RTO 1024) from Rohde & Schwarz. The Equipment Under Test (EUT), i.e., the capacitive sensing circuit, is positioned on a non-conductive bench above the ground plane. The LISN and the power supply are placed alongside the ground plane. The measurement instruments are placed outside the semi-anechoic chamber.

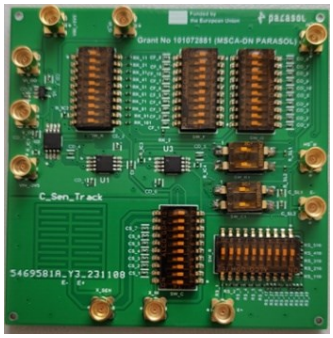

Fig. 5 Fabricated PCB of Capacitive touch sensing circuit.

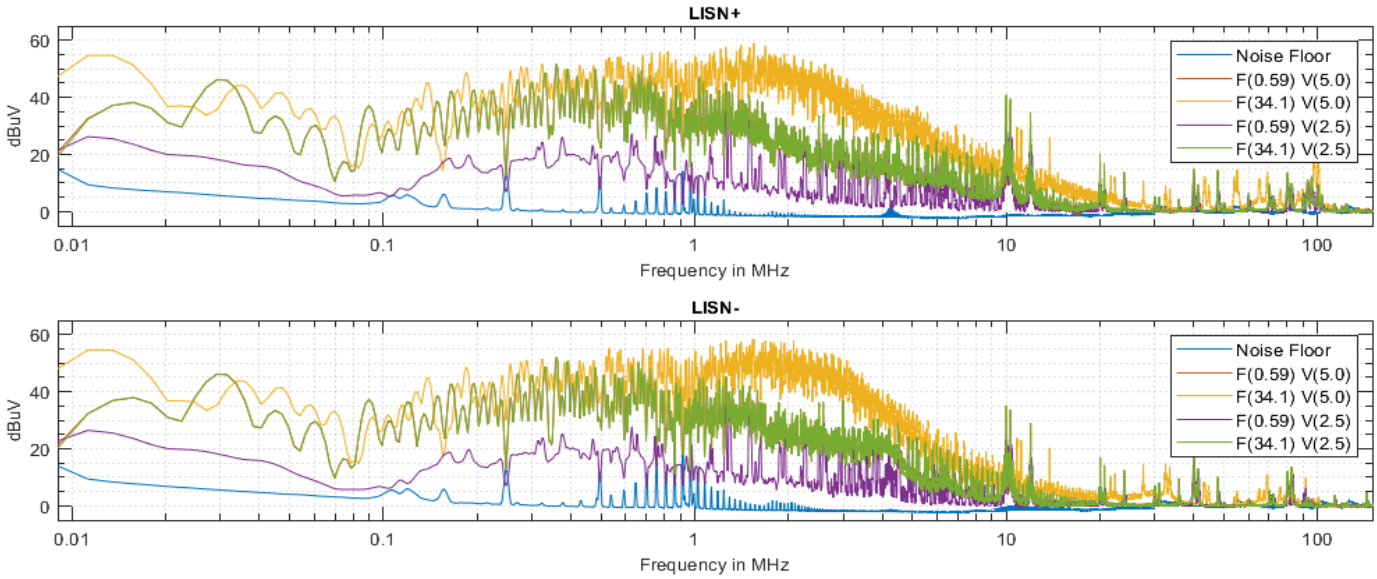

Fig. 7 Conducted Emission Frequency Domain Results.

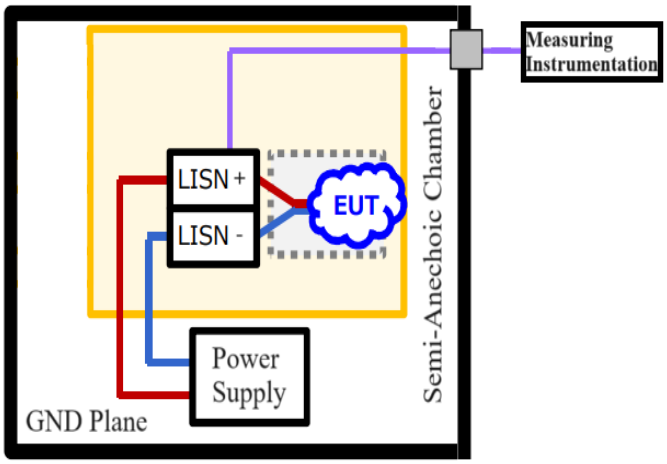

Fig. 6 Conducted EMI test setup.

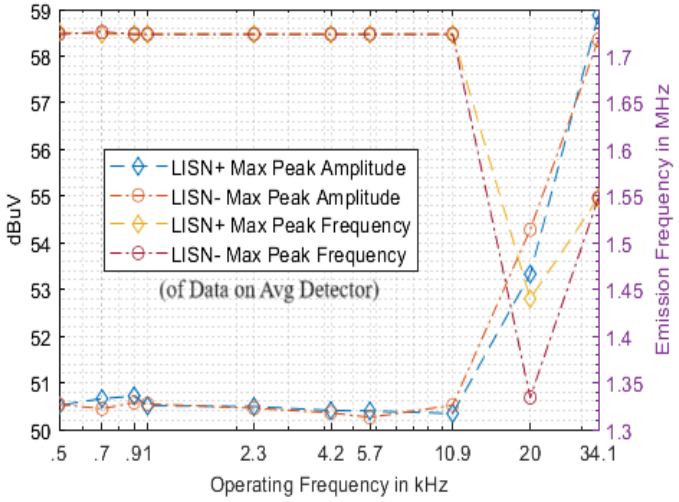

Fig. 8 EuT Operating Frequency versus Emission amplitude and frequency.

III. Results and Analysis

A. Conducted Emission in the Frequency Domain

The EMI test receiver is configured with:

- the frequency range between 9kHz to 150MHz,
- a resolution Bandwidth (RBW) of 9kHz,
- and the average detector is used.

Fig 7 shows the emissions data for the EuT at its maximum and minimum operating frequencies and voltages. Fig 8 demonstrates how the peak of the average emissions varies when the EuT's operational frequency changes, with the peak-peak operating voltage maintained constant at 5 V, and also shows the corresponding changes in emission frequency.

Likewise, Fig 9 illustrates the changes in peak average emissions when the operating voltage of the EuT is varied while keeping the operating frequency constant at 34.1kHz. It also shows the subsequent changes in emission frequency.

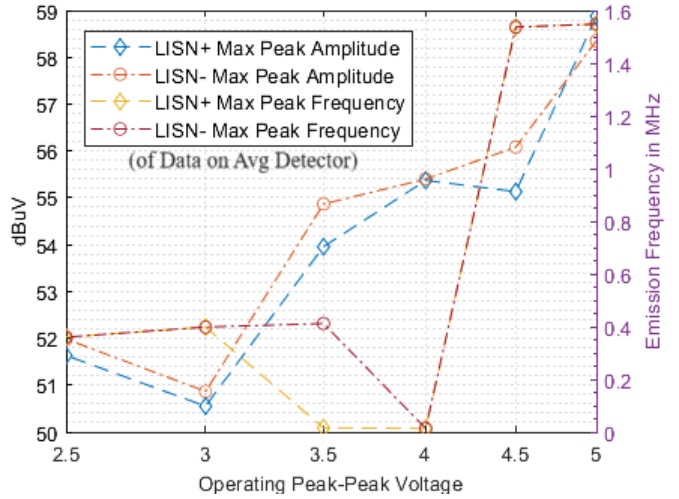

Fig. 9 EuT Operating Voltage versus Emission amplitude and frequency.

B. Conducted Emission in the Time Domain

The analysis presented includes the assessment of the output voltage V_{do}, integrator output V_i, zero-crossing detector output X_b, and oscillator output X_a. Fig 10 showcases the waveforms of these signals from the EuT, and Fig 11 shows corresponding waveform outputs from the LISNs.

In the experimental arrangement, the time-domain voltages across the 50Ω load from the LISNs are captured, with the parameters in Table 3. Furthermore, signals from the two different LISNs are recorded concurrently to minimize measurement errors or inconsistencies while maintaining the same setup environment used for frequency domain measurements.

Table 3 Time-domain acquisition specifications

Total recorded length	8ms
Acquisition Speed	5GSamples/s
Time Resolution	200ps
Total Samples	40e6
Input Impedance	50Ω

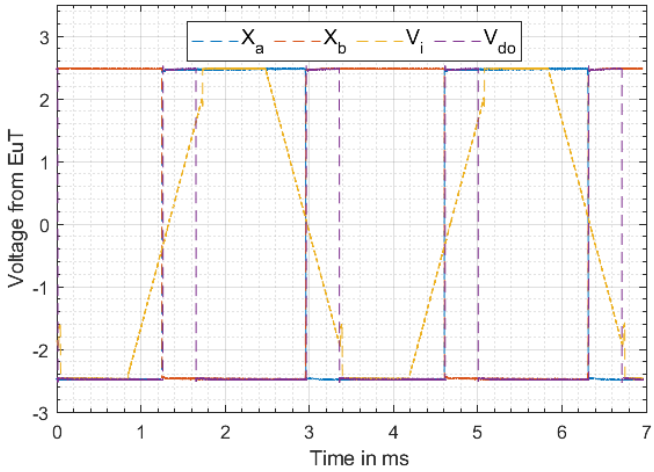

Fig. 10 Time-domain waveforms from EuT operating at F = 0.59 and V = 5.0.

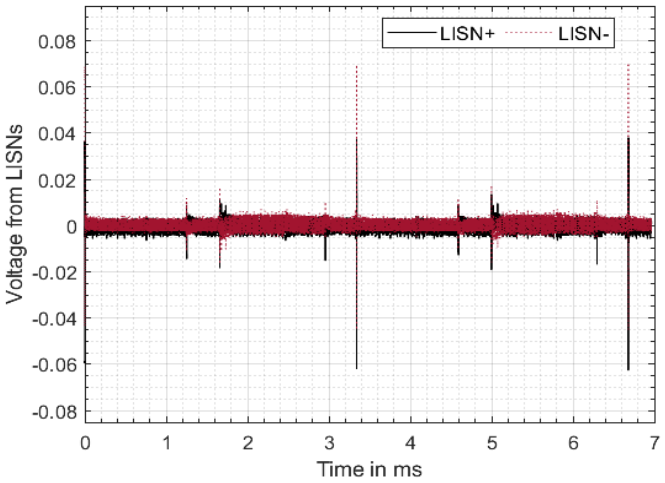

Fig. 11 Time-domain waveforms from LISNs when EuT operates at F = 0.59 and V = 5.0.

Fig 12 represents the time-frequency behavior of the common mode voltage calculated from the results of the time-domain signals from the LISN networks. For determining time-frequency domain results, a short-time Fourier transform is used with the parameters shown in Table 4 [14], [15].

Table 4 Time-Frequency domain analysis parameters

Parameters	Values
Window	Blackman-Harris
Resolution Bandwidth R_{BW}	9kHz
Nyquist Sampling[a] S_{NF}	300MHz
Window Length W_L	$W_L = {R_{BW}}^{-1}/{S_{NF}}^{-1}$
Overlapping	90%

[a] For faster calculation, recorded signals are down-sampled to 300MHz.

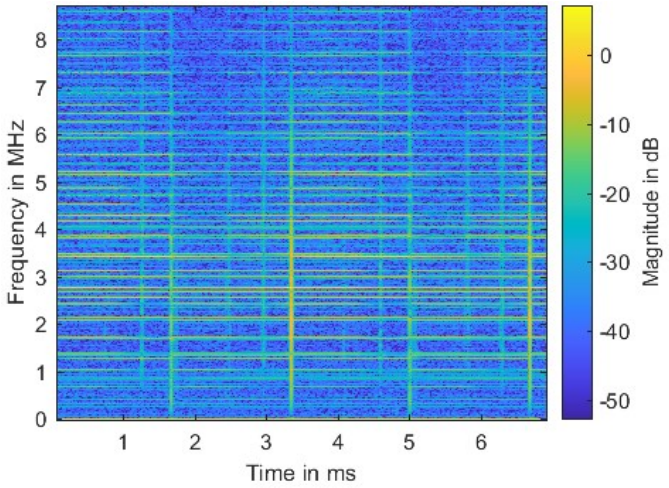

Fig. 12 Short-time Fourier Transform of common mode emission.

The time-domain results indicate that the transitions occurring during the charging and discharging of the integrating and sensing capacitor are major contributors to conducted emissions. Therefore, modifications in the design that decrease the total charge time, or the capacitance could reduce emissions while allowing for a higher frequency to maintain improved touch sensing speed.

IV. Conclusion

This research analyzes the conducted emission behavior of a self-oscillating capacitive touch-sensing circuit, revealing that an increase in the circuit's operating frequency leads to higher emission amplitudes. Similarly, an increase in the operating voltage of the sensing circuit results in amplified emissions. Traditional capacitive touch sensing circuits, such as sigma-delta capacitive sensing, require higher operating frequencies for enhanced sensing speed and accuracy, potentially generating more emissions. In contrast, the proposed sensing methodology employs changes in the time shift or phase of oscillation to detect capacitance variations. The effectiveness of this method in terms of speed, accuracy, and resolution centers on the acquisition or processing system's capability to discern minor variations in the phase or time shift of the output signal.

The study indicates that the minimization of conducted emissions is achievable through the efficient use of operating frequency and voltage at lower levels. Although, there is potential for enhancement in the discussed circuit design, particularly in reducing operating frequency and voltage. Transitioning from printed circuit-based self-oscillating capacitive sensing or analogous designs to very large-scale integration or integrated circuit platforms could facilitate a more effective sensing interface while maintaining reduced voltage and frequency requirements.

Ongoing research explores this methodology for multi-touch applications, including investigating the circuit's radiated emissions and susceptibility. These aspects are being carefully examined because lower operating voltages and frequencies might reduce radiated emissions.

REFERENCES

[1] S. Malik, L. Somappa, M. Ahmad, T. Islam, and M. S. Baghini, "An accurate digital converter for lossy capacitive sensors," *Sens Actuators A Phys*, vol. 331, Nov. 2021, doi: 10.1016/j.sna.2021.112958.

[2] S. Malik, L. Somappa, M. Ahmad, and M. S. Baghini, "An Accurate Auto-Tunable Quadrature-Phase Generator Circuit for Robust Sensing Applications," in *2020 IEEE 17th India Council International Conference, INDICON 2020*, Institute of Electrical and Electronics Engineers Inc., Dec. 2020. doi: 10.1109/INDICON49873.2020.9342500.

[3] M. Mathur, J. K. Rai, and N. Sridhar, "Electromagnetic compatibility analysis of projected capacitive touch technology based panel computer for military application," *J Electromagn Waves Appl*, vol. 30, no. 13, pp. 1689–1701, 2016, doi: 10.1080/09205071.2016.1211559.

[4] K. Wang, R. Mitev, C. Yan, X. Ji, A.-R. Sadeghi, and W. Xu, "Analyzing and Defending GhostTouch Attack against Capacitive Touchscreens," *IEEE Trans Dependable Secure Comput*, pp. 1–16, 2024, doi: 10.1109/TDSC.2024.3352593.

[5] Y. Li, S. Wang, H. Sheng, C. P. Chng, and S. Lakshmikanthan, "Investigating CM Voltage and Its Measurement for AC/DC Power Adapters to Meet Touchscreen Immunity Requirement," *IEEE Trans Electromagn Compat*, vol. 60, no. 4, pp. 1102–1110, Aug. 2018, doi: 10.1109/TEMC.2018.2794318.

[6] P. Vooka and B. George, "A Direct Digital Readout Circuit for Impedance Sensors," *IEEE Trans Instrum Meas*, vol. 64, no. 4, pp. 902–912, 2015, doi: 10.1109/TIM.2014.2361552.

[7] P. Vooka and B. George, "An improved capacitance-to-digital converter for leaky capacitive sensors," *IEEE Sens J*, vol. 15, no. 11, pp. 6238–6247, Nov. 2015, doi: 10.1109/JSEN.2015.2454531.

[8] P. Vooka and B. George, "A Method for Improving Conversion Rate and Accuracy of a Capacitance-to-Digital Converter."

[9] Yŏnse Taehakkyo, IEEE Electromagnetic Compatibility Society, Han'guk Chŏnjap'a Hakhoe, and Institute of Electrical and Electronics Engineers, *2017 Asia-Pacific International Symposium on Electromagnetic Compatibility (APEMC 2017) : June 20-23, 2017, the Commons, Yonsei University, Seoul, Korea*.

[10] B. Zhang and S. Wang, "Analysis of the Susceptibility of Capacitive Touchscreens to External Electric Field Interference," in *2022 Asia-Pacific International Symposium on Electromagnetic Compatibility, APEMC 2022*, Institute of Electrical and Electronics Engineers Inc., 2022, pp. 739–741. doi: 10.1109/APEMC53576.2022.9888500.

[11] S. Malik, M. Ahmad, S. Laxmeesha, T. Islam, and M. S. Baghini, "Impedance-to-time converter circuit for leaky capacitive sensors with small offset capacitance," *IEEE Sens Lett*, vol. 3, no. 7, Jul. 2019, doi: 10.1109/LSENS.2019.2919894.

[12] C. Riener *et al.*, "Broadband Modeling and Simulation Strategy for Conducted Emissions of Power Electronic Systems Up to 400 MHz," 2022, doi: 10.3390/electronics.

[13] A. N. Lemmon, A. D. Brovont, C. D. New, B. W. Nelson, and B. T. Deboi, "Modeling and Validation of Common-Mode Emissions in Wide Bandgap-Based Converter Structures," *IEEE Trans Power Electron*, vol. 35, no. 8, pp. 8034–8049, Aug. 2020, doi: 10.1109/TPEL.2019.2963883.

[14] J. O. Smith, "Spectral Audio Signal Processing," *Center for Computer Research in Music and Acoustics (CCRMA)*, pp. 1–674, 2011, Accessed: Feb. 20, 2024. [Online]. Available: https://ccrma.stanford.edu/~jos/sasp/

[15] "Invertibility of overlap-add processing." Accessed: Feb. 20, 2024. [Online]. Available: https://gauss256.github.io/blog/cola.html